ChemPhysChem

Research Article
doi.org/10.1002/cphc.202200012

**Chemistry
Europe**
European Chemical
Societies Publishing

www.chemphyschem.org

Introducing Alternative Algorithms for the Determination of the Distribution of Relaxation Times

Tobias G. Bergmann[a] and Nicolas Schlüter*[b]

Impedance spectroscopy is a powerful characterization method to evaluate the performance of electrochemical systems. However, overlapping signals in the resulting impedance spectra oftentimes cause misinterpretation of the data. The distribution of relaxation times (DRT) method overcomes this problem by transferring the impedance data from the frequency domain into the time domain, which yields DRT spectra with an increased resolution. Unfortunately, the determination of the DRT is an ill-posed problem, and appropriate mathematical regularizations become inevitable to find suitable solutions.

The Tikhonov algorithm is a widespread method for computing DRT data, but it leads to unlikely spectra due to necessary boundaries. Therefore, we introduce the application of three alternative algorithms (Gold, Richardson Lucy, Sparse Spike) for the determination of stable DRT solutions and compare their performances. As the promising Sparse Spike deconvolution has a limited scope when using one single regularization parameter, we furthermore replaced the scalar regularization parameter with a vector. The resulting method is able to calculate well-resolved DRT spectra.

1. Introduction

Electrochemical impedance spectroscopy (EIS) is essential for analyzing a variety of electrochemical systems. EIS can be used for the investigation of reaction mechanisms,[1,2] fuel cells,[3,4] microbial fuel cells,[5–7] batteries,[8–10] corrosion processes,[11,12] and other systems.[13,14] Being fast, cost-effective, and non-invasive, EIS is an advantageous technique.

In general, an impedance experiment is performed within a broad user-chosen frequency range. Therefore, the measured impedance spectrum reflects a combination of various overlapping physical-chemical effects which determine the electrochemical behavior of the investigated system. The challenge of an EIS analysis is now to interpret the obtained impedance spectrum correctly. A common approach to evaluate experimental impedance spectra is to approximate the investigated system by electrical equivalent circuits (EC) as fitting models. The equivalent circuits generally contain passive electrical components like resistors, capacitors, inductors, and Warburg impedances and should represent the studied electrochemical systems as well as possible. After mathematically fitting the impedance behavior of the equivalent circuits to the experimental impedance spectra, these models can be used to estimate the parameters of the electrochemical system like the resistance of charge transfer processes.[15] However, often various ECs can be used to describe and fit a specific impedance spectrum, which can make impedance studies ambiguous and elaborate.[2]

In this work, we assume that a preprocessing of a certain impedance spectrum may eliminate any inductive and diffusive impedance behavior (the latter can be described by Warburg impedances).[16,17] The remaining spectrum can then solely be described and fitted using RC-circuits (parallel connection of a resistor and a capacitor) connected in series. Herein the RC-circuits represent polarization processes (e.g., charge transfer processes). This way, the simplified impedance Z can be represented as,

$$Z = Z_{RC,1} + Z_{RC,2} + Z_{RC,3} + ... + Z_{RC,N} \qquad (1)$$

and the impedance of each RC-circuit $Z_{RC,i}$ is calculable by

$$Z_{RC,i} = \frac{R_i}{1 + jR_iC_i\omega} = \frac{R_i}{1 + j\tau_i\omega}. \qquad (2)$$

R_i is the resistance, and C_i is the capacitance of the respective RC-circuits. ω is the angular frequency of the alternating excitation signal (electrical current or voltage), τ_i is the time constant of the individual RC-circuits, and j is the imaginary unit.

Commonly, the impedance behavior of electrochemical systems cannot be entirely described by ideal passive elements. Because of uneven and porous electrode surfaces or other inhomogeneities, the electrochemical double layer formation does not correspond to the charging of an ideal capacitor.[18] Therefore, the capacitor is replaced by a Constant-Phase-Element (CPE), and the RC-element is replaced by the ZARC-element. The impedance of the ZARC-element is then given by,[15,19]

[a] T. G. Bergmann
Institute of Environmental and Sustainable Chemistry,
Technische Universität Braunschweig, Braunschweig, Germany
[b] Dr. N. Schlüter
Institute of Energy and Process Systems Engineering,
Technische Universität Braunschweig, Braunschweig, Germany
E-mail: nicolas.schlueter@tu-bs.de

ChemPhysChem

Research Article
doi.org/10.1002/cphc.202200012

Chemistry Europe
European Chemical
Societies Publishing

$$Z_{\mathrm{ARC},i} = \frac{R_i}{1 + (j\tau_i\omega)^{P_i}}. \tag{3}$$

P_i is an exponential parameter that describes the deviation of the CPE from an ideal capacitor. Given that $0 \leq P \leq 1$. Accordingly, the CPE has a phase angle of $-P_i\frac{\pi}{2}$.[18,20] The time constant τ_i is now given by,

$$\tau_i = Q_i \cdot \sqrt[P_i]{R_i} \tag{4}$$

where Q_i has no clear physical meaning for $P\neq 1$.[21] For $P = 1$ the CPE corresponds to a capacitor. In this paper, the parameter Q will be called the CPE coefficient.

For a user-chosen number N of ZARC-elements (each representing an electrochemical polarization process), the experimental impedance data can be fitted and analyzed using various methods.[22–24] Here, the standard method is an CNLS (complex non-linear regression least-squares) fitting. Al-Ali et al. show in [24] an interesting alternative approach to quantify impedance data. However, the challenging problem is that many polarization processes occur in overlapping frequency domains.[25] Hence, a reasonable estimation of N can become complicated. A wrong number N oftentimes still reproduces the qualitative shape of the experimental impedance spectrum but leads to miserable fitting values for the determined parameters of the ZARC-elements. For a better estimation of N, the frequency-dependent impedance spectrum can be transferred into a non-negative time-dependent distribution function, the so-called distribution of relaxation times (DRT). Like every probability distribution or density function, the DRT is non-complex and positive. The DRT-method was introduced by Schweidler.[26]

It holds that

$$Z(\omega) = \int_{-\infty}^{\infty} \frac{\gamma(\ln(\tau))}{1 + j\omega\tau} \, d\ln(\tau), \tag{5}$$

which corresponds to a Fredholm integral equation.[27] Here, $\gamma(\ln(\tau))$ is a positive spectrum with

$$\int_{-\infty}^{\infty} \gamma(\ln(\tau)) \, d\ln(\tau) = \sum_i^N R_i. \tag{6}$$

R_i are the resistances of the individual ZARC-elements. For a known model for Z (number N of ZARC-elements and all parameters of the passive elements are given) the equation 5 is analytically solvable.[28] The corresponding DRT spectrum for a single ZARC-element is given by,[16,19]

$$\gamma(\ln(\tau)) = \frac{R}{2\pi} \frac{\sin(P\pi)}{\cosh(P(\ln(\tau_0) - \ln(\tau))) + \cos(P\pi)}, \tag{7}$$

τ_0 is the time constant of the ZARC-element and can be calculated with the resistance R, the CPE coefficient Q and the exponent P using equation 4. The equation 7 looks similar to a normal distribution and has a maximum for $\tau = \tau_0$. Accordingly,

the DRT spectrum of an impedance spectrum, which is based on multiple ZARC-elements, contains multiple peaks. In the DRT spectrum, each peak represents one ZARC-element.

The DRT spectrum has a higher resolution than the corresponding impedance spectrum, and hence it is suitable to find the optimal number of ZARC-elements within the EC.[29] Determining the DRT from experimental impedance data, however, requires the solution of an ill-posed problem. Ill-posed problems have infinite possible solutions and hence require special mathematical treatments like regularizations to prevent overfitting. The direct analytical DRT solution for experimental impedance data is prone to instabilities like too many peaks or oscillations in the resulting DRT spectrum.[30] The ill-posed problem of the DRT method is commonly solved by operating a Fourier transformation[31,32] or by using a Tikhonov regularization.[33] Nevertheless, it could be shown, that it is impossible to get the true DRT by utilizing a Fourier transformation.[32] The Tikhonov regularization, in turn, has the disadvantage that the solution includes positive and negative values if no boundaries are chosen. Boundaries, on the other hand, yield a poor DRT resolution or too many peaks. The usage of alternative regularizations could overcome the problems accompanied by the Tikhonov method. Here, the Gold and the Richardson-Lucy deconvolution are promising, as they do not need boundaries under specific conditions.[34,35] The Sparse Spike deconvolution is less popular but has the advantage that the calculated DRT is directly presentable as a sum of ZARC-elements. Thus, we compare the often used Tikhonov approach with the beforehand mentioned regularizations in this work. Here, the various algorithms are applied to different impedance simulations to compare their performance. Besides, we present a novel method based on the Sparse Spike deconvolution, where we replaced the regularization parameter with a regularization vector for calculating an almost perfect DRT.

The scope of this work is to shortly introduce all algorithms, and to show that besides the Tikhonov regularization alternatives exist, which may achieve better results for DRT investigations. The details of the algorithms studied in this work can be found in the references given for each algorithm, respectively. After introducing the various algorithms (cf. section 2), the different approaches will be benchmarked according to their accuracy to describe DRT spectra from experimental impedance data (cf. section 3.2). For this purpose, simulated EIS data are used because for the synthetic data we can obtain the theoretical DRT solution. This allows a straightforward comparison of the DRT solutions determined with the different algorithms with the theoretically optimal DRT spectrum. The studied impedance test data and the utilized criteria to rate the performance of each algorithm are introduced in section 3.1. Eventually, the promising Sparse Spike Deconvolution was revised to yield more accurate DRT results. The respective discussion can be found in section 3.3.

ChemPhysChem

Research Article
doi.org/10.1002/cphc.202200012

**Chemistry
Europe**

European Chemical
Societies Publishing

2. Theory

2.1. The Ill-Posed Problem

The calculation of the DRT with equation 5 from experimental impedance data is an ill-posed problem. Accordingly, slight measurement errors in Z have a large influence on the resulting DRT. Erroneous impedance data can lead to additional peaks in the DRT, for example. This effect can be prevented by operating regularizations.

By using matrix notation, the equation 5 can be transposed into the following form:[36]

$$Z = \mathbf{A}x, \tag{8}$$

herein the impedance $\mathbf{Z}$ and the Toeplitz matrix $\mathbf{A}$ are complex. The DRT $\mathbf{x}$, on the other hand, is a positive non-complex vector. Therefore, this equation can be divided into

$$\mathbf{Z}' = \mathbf{A}'\mathbf{x}, \tag{9}$$

and

$$\mathbf{Z}'' = \mathbf{A}''\mathbf{x}, \tag{10}$$

where $\mathbf{Z}'$ is the real and $\mathbf{Z}''$ is the imaginary part of $\mathbf{A}$. can be computed according to the works of Wan et al. and Gavrilyuk et al.[36,37] The DRT $\mathbf{x}$ can be calculated with equations 9 and 10. As both these equations represent ill-posed problems, regularizations are needed.

Most regularizations use a scaling parameter (i.e., regularization parameter) that prevents overfitting. This parameter can smooth the results, reduce the norm of the results, or cause an early stopping for iterative algorithms, for instance. However, the regularization parameter needs to be prechosen by the user. Validation methods can help to find an optimal parameter value.[38] In this context, optimal means that the regularized solution describes the problem as accurately as possible and that the results are neither overfitted nor underfitted. In this work, we use a validation method introduced by Saccoccio et al.[39] The Re–Im cross-validation (RICV) starts with calculating the DRT from the real impedance part $\mathbf{x}_1$ (or from the imaginary impedance part $\mathbf{x}_2$, respectively). In the following step, the resulting DRT spectrum is used to recalculate impedance information in the frequency domain using equations 9 and 10. The recalculated imaginary impedance (or the real part, respectively) is then compared to the imaginary part (or the real part, respectively) of the pristine experimental impedance $\mathbf{Z}_{sim}$.

$$RICV = \left\|\mathbf{Z}'_{sim} - \mathbf{A}'\mathbf{x}_2\right\|_2 + \left\|\mathbf{Z}''_{sim} - \mathbf{A}''\mathbf{x}_1\right\|_2 \tag{11}$$

In the results of this paper, we will present the norm of the imaginary part and the norm of the real part separately.

For the general treatment of the algorithms, we use an ill-posed problem of the generalized form,

$$Z = A \cdot x. \tag{12}$$

2.2. Tikhonov Regularization

The Tikhonov regularization is a common approach for computing the DRT. The fundamental equation is given by,[40]

$$\min_{x \geq 0}(\|Z - A \cdot x\|_2 + \lambda\|L \cdot x\|_2). \tag{13}$$

The first term resembles a linear least-squares approach. For ill-posed problems, this term alone would strongly overfit the data. The second term is a penalty term, which prevents overfitting. Here λ is the regularization parameter that scales this term. L is an identity matrix, the first or the second numerical derivative operator.[40] Many works used this algorithm for the calculation of the DRT,[41–43] and several approaches were developed to calculate the optimal λ.[30,37,38,41,44] This regularization leads to a DRT with positive and negative values, but the DRT must be positive as explained above. Therefore, constraints are essential to eliminate the negative values to get suitable spectra.[45] Unfortunately, constraints can also deteriorate the results. This problem will be discussed in chapter 4. The Tikhonov regularization and its impact on the solution are well documented in [46].

2.3. Gold Deconvolution

The Gold deconvolution is an extension of the Van-Cittert deconvolution introduced in [35]. The Gold deconvolution is a non-negative iterative method for regularizing ill-posed problems. The Van Cittert iteration is given by,[47,48]

$$x^{k+1} = x^k + \mu \cdot \left((A^TAA^T)Z - Hx^k\right), \tag{14}$$

with

$$H = (A^TAA^TA). \tag{15}$$

Here, μ is a relaxation factor. In the Gold deconvolution, the relaxation factor is given by [45] as

$$\mu_i = \frac{x_i^k}{\sum_m (H_{i,m})x_m^k}. \tag{16}$$

Hence, the Gold iteration is described as

$$x_i^{k+1} = x_i^k \frac{(A_i^TAA^T)Z}{\sum_m (H_{i,m})x_m^k}. \tag{17}$$

If the spectrum f and the impulse response function A own the same sign, the result x is always positive. Accordingly, this method does not need constraints and is very suitable for deconvolution in spectroscopic methods.[45,49] The Gold decon-

ChemPhysChem

Research Article
doi.org/10.1002/cphc.202200012

**Chemistry
Europe**
European Chemical
Societies Publishing

volution is an iterative algorithm, and thus, the results are underfitted for too small iteration numbers, and for too high iteration numbers, the results are overfitted. Hence, this method is regularized by an early stopping of the algorithm. Here, the regularization parameter is the iteration maximum.

2.4. Richardson Lucy Algorithm

The Richardson Lucy (RL) deconvolution resembles the Gold deconvolution. In addition, the Richardson Lucy deconvolution requires a point spread function (PSF),[50] which often corresponds to the convolution matrix of the problem and has a matrix norm of 1. The RL deconvolution is often used for image deblurring, where the PSF corresponds to the kernel of the image.[48,51] For calculating the DRT, the PSF is given by,

$$P = \frac{-A_{im}}{||A_{im}||_2}.$$ (18)

The iteration is given by,[48,52]

$$x_i^{k+1} = x_i^k \cdot \sum_n P_{n,i} \cdot \frac{Z_n}{\sum_j (A_{n,j}) x_j^k}.$$ (19)

As for the Gold iteration, the result x is always positive, and the algorithm does not need any constraints. By comparing the equation of the RL deconvolution and the Gold iteration, it can be seen that the fraction of the Gold iteration is expanded by multiple matrices of A. In section 3.2, we will show that this expansion leads to a higher needed iteration number for the Gold algorithm. For more details, further works can be recommended that also compare and analyze results of the RL and the Gold deconvolution (e.g. [48,53]).

2.5. Sparse Spike Deconvolution

The Sparse Spike deconvolution (SSD) is a method, which is popular in seismology.[50,54–57] In our case, the assumption is made that the DRT spectrum x is composed of a certain number of sparse peaks c_m, which all own the same impulse function G:

$$x_i = \sum_m^M G_{i,m}(P) c_m = G_i(P) \cdot c.$$ (20)

This equation leads to the following minimization,

$$\min_{c \geq 0}(||Z - A \cdot G(P) \cdot c||_2),$$ (21)

where P is the regularization parameter and determines the width of the impulse function G. The constraint $c \geq 0$ is essential to get a suitable spectrum. In seismology, a constant source impulse function is well known but the experimental data are highly erroneous. Therefore, an additional Lasso regularization is often used to prevent overfitting.[54] In our case,

unlike in seismology, an additional regularization should not be necessary because the experimental data are assumed to be only slightly erroneous. The DRT spectrum is expected to be composed of many ZARC-elements. Hence, we use the optimal DRT function for a ZARC-element (see equation 7) as the impulse function. Accordingly, for a spectrum consisting of m time constants, the impulse function for the time constant τ_i is represented by

$$g_{i,m}(P) = \frac{1}{2\pi} \frac{\sin(P\pi)}{\cosh(P(\ln(\tau_i) - \ln(\tau_m))) + \cos(P\pi)}.$$ (22)

Subsequently, every column is normalized by

$$G_{i,m}(P) = \frac{g_{i,m}(P)}{\sum_i(g_{i,m}(P))}.$$ (23)

If the system contains ZARC-elements which all have the same parameter P, one impulse function G can be chosen so that an optimal x is calculable with equation 20 after the minimization of equation 21.

A short overview of the main properties of all algorithms introduced beforehand is given in Table 1. Here, the constraints and the utilized regularization parameters are listed. Furthermore, information is given whether the algorithms are iterative or non-iterative.

3. Results

3.1. Test Data Sets and Performance Citeria

Simulated erroneous impedance spectra of ZARC-elements have been used to determine DRT spectra with the beforehand introduced algorithms and to benchmark the algorithms. In this work, we focus on synthetic impedance spectra to compare the calculated DRT with the optimal one. The latter is only accessible for simulated data where all impedance information, including the exact equivalent circuit used for the computation of the EIS data, is given. For experimental impedance spectra, on the other hand, the optimal DRT remains unknown. Four different simulations were considered. The first spectrum consists of three broad overlapping ZARC-signals with a low error rate. The second spectrum also represents three ZARC-elements but with varying CPE coefficients and high error rates. The impedance spectra and the corresponding analytical DRT

Table 1. Properties for the algorithms.

Algorithms	Constraints	Reg. parameter	Type
Tikhonov	$x \geq 0$	λ	non-iterative
Gold	not needed	iteration number	iterative
Richardson Lucy	not needed	iteration number	iterative
Sparse Spike Deconvolution	$c \geq 0$	P	non-iterative

ChemPhysChem

Research Article
doi.org/10.1002/cphc.202200012

Chemistry Europe
European Chemical
Societies Publishing

spectra, which are calculated by equation 7, are presented in Figure 1. To show the influence of the error solely, we calculated a third simulation, where we used the impedance parameters of the first simulation and increased the super-imposed error. The respective results for varied errors are presented in the Supporting Information (7). In a fourth simulation, we investigated the influence of the resistance magnitude and the number of passive elements within the equivalent circuits on the performance of the algorithms. Thereby, we eliminated the last RCPE element in the equivalent circuit of the second impedance simulation and divided all resistances by a factor of 1000. The results of these investigations are presented in the Supporting Information (7).

All simulation parameters are listed in the Experimental Section.

The DRT results of the various algorithms were validated by comparing them with the corresponding analytical DRT spectrum by,

$$\nu = ||\mathbf{x} - \mathbf{x}_{best}||_2. \tag{24}$$

Here, ν represents the DRT quality by comparing the experimental results (depending on the algorithm used) to the theoretically optimal DRT spectrum $\mathbf{x}_{best}$. A low ν indicates an estimated DRT spectrum close to the optimal.

Besides minimal ν values, it is important that the DRT solutions can be reconstructed into appropriate impedance data that match the initial experimental EIS data as closely as possible. Therefore, we compare impedance spectra recalcu-

lated from the computed DRT solution and EIS data that is based on the optimal DRT spectrum $\mathbf{x}_{best}$. To interpret the DRT spectra's quality and the used algorithm's eligibility, we estimate these impedance spectra by using equation 8 and calculate,

$$\mu = ||A_{im} \cdot \mathbf{x} - A_{im} \cdot \mathbf{x}_{best}||_2 + ||A_{re} \cdot \mathbf{x} - A_{re} \cdot \mathbf{x}_{best}||_2 \tag{25}$$

A small μ indicates an algorithm leading to a DRT, which can reproduce the experimental impedance spectrum and is hence not underfitted. Unfortunately, an overfitted DRT also shows a small μ value. But in this case, the overfitted DRT should lead to a high ν.

The real part of the impedance (see equation 9) or the imaginary part (see equation 10) can be used for calculating the DRT. We will calculate both results and will present them side by side.

Additionally, to compare and rate the final DRT spectra, we determined the Tanimoto distance to the optimal DRT by

$$t = 1 - \left(\frac{\mathbf{x} \cdot \mathbf{x}_{best}}{||\mathbf{x}||_2^2 + ||\mathbf{x}_{best}||_2^2 - \mathbf{x} \cdot \mathbf{x}_{best}} \right) \tag{26}$$

If the DRT spectra $\mathbf{x}$ and $\mathbf{x}_{best}$ are identical, we get a Tanimoto distance of 0. But if the spectra have no overlapping areas, the Tanimoto distance will be 1.[58] Besides the quality of the DRT outcomes of each algorithm, we also considered the calculation times that are associated with the various approaches.


(a)

(b)

(c)

(d)
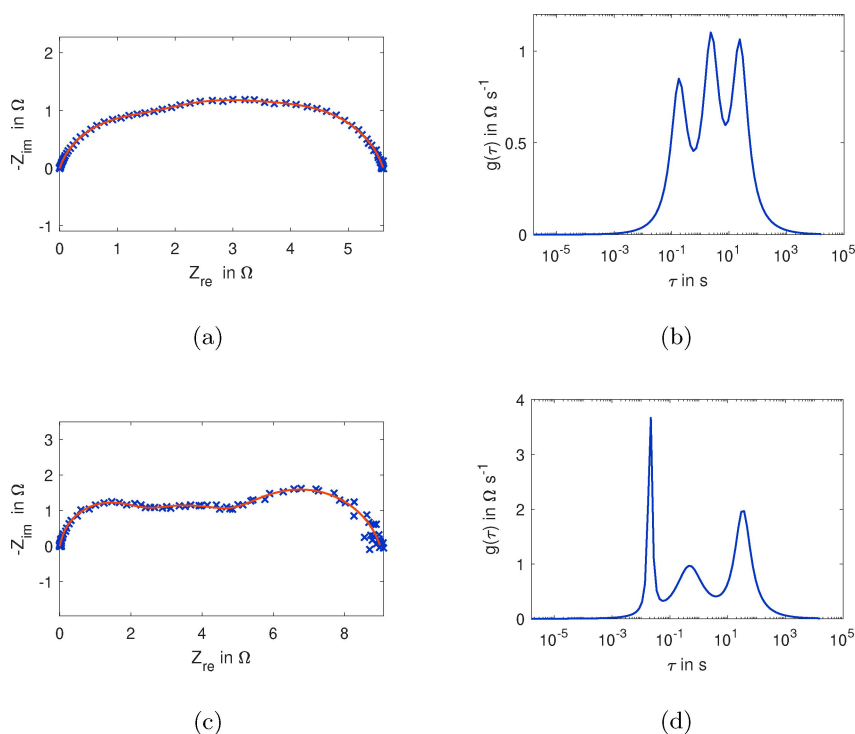
Figure 1. Nyquist plot of the first simulation (a) and the second simulation (c). The optimal DRT for the first Nyquist-Plot (b) and for the second Nyquist-Plot (d). The upper DRT shows that the Nyquist-Plot contains three ZARC-elements with strongly overlapping semicircles. In the lower DRT is the influence of the variant exponents P apparent.

ChemPhysChem

Research Article
doi.org/10.1002/cphc.202200012

Chemistry Europe
European Chemical
Societies Publishing

3.2. Comparison of the Algorithms

For each algorithm, the determination of the DRT depends on a regularization parameter (cf. Table 1), which should prevent over- and underfitting. Herein, the previously introduced RICV can be calculated by equation 11 and used to estimate a suitable regularization parameter. To compare the results of the algorithms with each other, we calculate ν and μ with equations 25 and 24 utilizing varying regularization parameters. For the Tikhonov regularization we used 1000 different λ values between 10^{-2} and 10^{-6} and for the Sparse Spike deconvolution,

we used 1000 different P values between 0.5 and 0.99. The iterative methods have been calculated up to 10^5 cycles.

In Figure 2, ν, μ and the corresponding RICV values are plotted for all algorithms applied to the first simulation setup of section 3.1. On the left side the imaginary part (equation 10) was used to calculate the DRT spectra. Accordingly, we calculated $RICV = \left\| \mathbf{Z}'_{sim} - \mathbf{A}' \mathbf{x}_2 \right\|_2$. On the right side, the real part (equation 9) and $RICV = \left\| \mathbf{Z}''_{sim} - \mathbf{A}'' \mathbf{x}_1 \right\|_2$ have been used. It can be seen that μ is almost always smaller when using the real part for each regularization. Accordingly, the accuracy of the recalculated impedance spectra is better when the real part is considered for calculating the DRT solution.
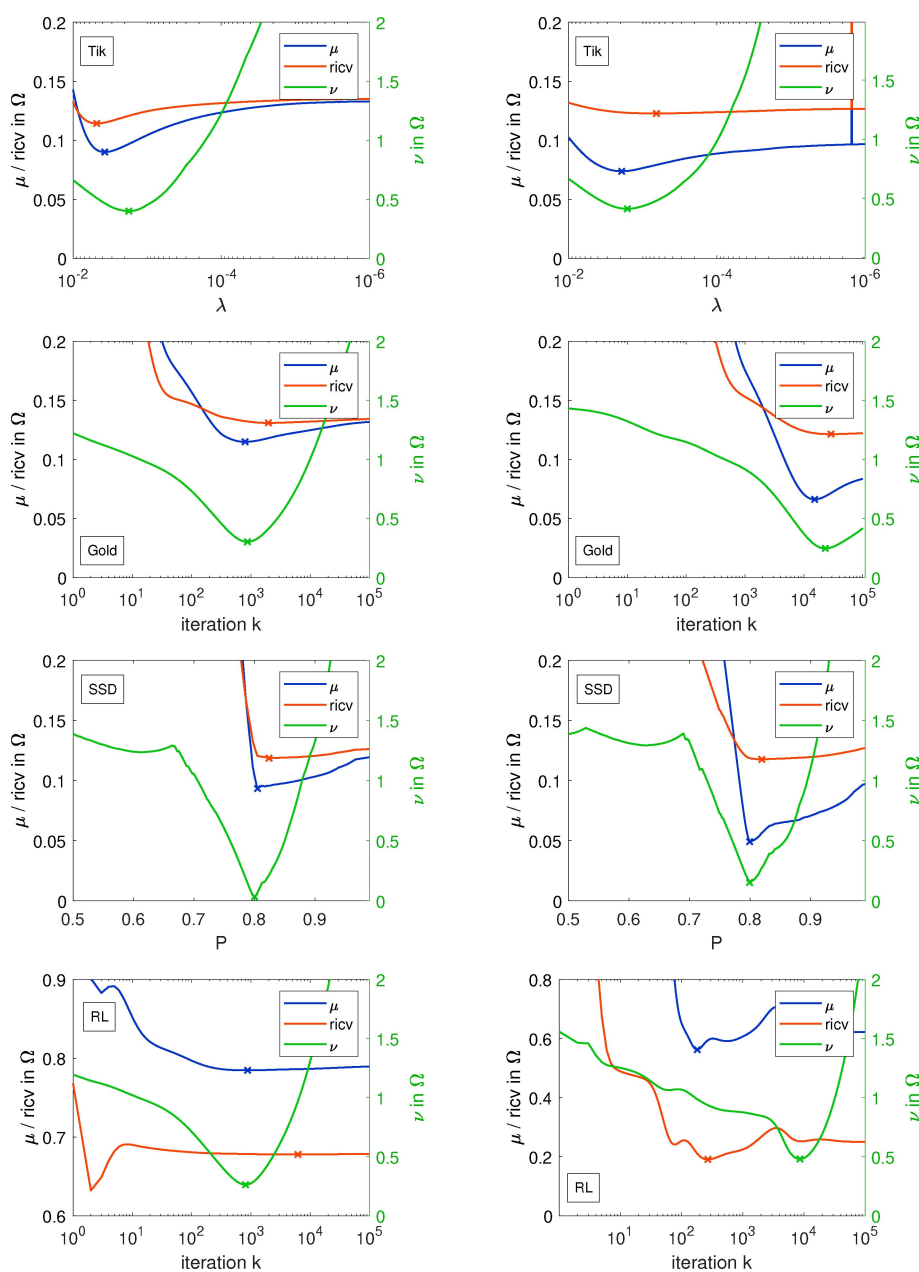
Figure 2. ν and μ plotted against the regularization parameter for the first simulation, computed with different algorithms. Each row represents one algorithm. From top to bottom the algorithms are: Tikhonov, Gold, SSD, Richardson-Lucy. The first column used the imaginary part (equation 10) and the second used the real part (equation 9) for the calculation.

ChemPhysChem

Research Article
doi.org/10.1002/cphc.202200012

**Chemistry
Europe**
European Chemical
Societies Publishing

The Tikhonov regularization shows good results for $5 \cdot 10^{-3} \geq \lambda \geq 5 \cdot 10^{-4}$ for the real and the imaginary part respectively. The increasing μ for a large λ indicates underfitting and the increasing ν for small λ values implies overfitting. The best DRT solution (smallest ν) can be found for $\lambda = 1.8 \cdot 10^{-3}$ when using the imaginary part and for $\lambda = 1.6 \cdot 10^{-3}$ when using the real part. The DRT results are slightly worse when using the real part, but a smaller μ shows that the recalculated impedance spectra are better in this case. It is also worth noticing that the RICV's minimum does not match the minimum of μ or ν.

The Gold algorithm leads to better results than the Tikhonov regularization (lower ν values). When the real part is used higher iteration numbers are needed. The best ν can be found for around 20000 iterations when using the real part. For the imaginary part, on the other hand, a distinct ν minimum can be found at around 900 iterations. The best μ values are at slightly lower iteration numbers than the best ν values. For this example, the RICV minima are at slightly higher iteration numbers. Therefore, the RICV leads to a beginning overfitting.

The Sparse Spike deconvolution achieves the lowest μ values using the real impedance part within the DRT computation. If P is chosen too small, the spectrum can no longer be resolved properly, causing μ to increase drastically. This trend is observable, regardless of the computational basis of the DRT data (real or imaginary part). The RICV resembles the characteristic μ curve for both the real and the imaginary part. For the ν values, a clear minimum can be found in the region of the steep increase of μ. The μ and the ν test function show a minimum around $P = 0.8$. Interestingly, this value corresponds to the used exponents of the ZARC-elements within the simulation. The RICV indicates an optimum for slightly higher P values, which are still in good accordance with the other results.

The Richardson-Lucy algorithm shows very high μ values, regardless of the number of iterations completed. Hence, the impedance spectra which can be recalculated from the respective DRT data are highly inaccurate. Thus, this algorithm generally leads to an oversimplification of the solution and yields underfitted DRT spectra. The ν values, on the other hand, do not show any noticeable irregularities in comparison to the results of the other algorithms. In contrast to the results of the remaining algorithms, the Richardson-Lucy approach yields RICV values that lie below the respective μ values. In addition, no pronounced minimum can be found in the RICV curve for the Richardson-Lucy algorithm. The first ten iterations lead to miserable DRTs, therefore the minimum at the first iteration is to be ignored. In a nutshell, the overall high μ values indicate that the Richardson-Lucy algorithm is not suitable for calculat-

ing DRT spectra that can be recalculated into valid impedance data.

Overall the Sparse Spike deconvolution achieves the smallest ν and μ values. The Gold algorithm and the Tikhonov regularization have similar μ values, but the Gold algorithm achieves smaller ν outcomes than Tikhonov. The RICV can be used for all presented algorithms except the Richardson-Lucy algorithm to find optimal regularization parameters. However, oftentimes the RICV leads to slightly overfitted DRT spectra.

In Figure 3, a comparison of the DRT spectra, that have been computed with the various algorithms, and the theoretically optimal DRT are shown. Here, we used for all calculations the optimal regularization as indicated by the respective RICV values. The used regularization parameters, the calculation times, and the Tanimoto distances for all algorithms are listed in Table 2. All DRT spectra were calculated based on the real part. For the Richardson-Lucy deconvolution, the peaks are poorly resolved and overlap too strongly. Especially at higher time constants, the peaks merge. This insufficient peak separation again indicates an underfitting of the problem. The other algorithms can differentiate all three peaks properly. However, the Gold algorithm and the Tikhonov regularization yield a small additional peak at $\tau = 300$ s. Additional peaks (artifacts) are highly disruptive as they reduce the total resistance of the real peaks and can cause misinterpretation of the entire DRT outcome. Furthermore, oscillations in the range of low time constants ($\tau \leq 0.05$ s) are conspicuous for the Tikhonov and the RL regularization. Apart from the additional peak at $\tau = 300$ s, the Gold algorithm shows no oscillations. The
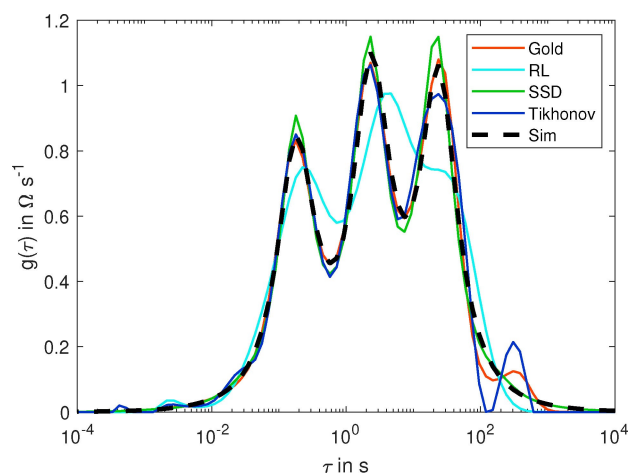
Figure 3. DRT spectra of all algorithms for the first simulation setup when the RICV is used for determining the regularization parameter. All DRT spectra were calculated from the real impedance part.

Table 2. Regularization parameters, calculation times, and Tanimoto distances to the optimal DRT for each DRT calculated by the various algorithm and shown in Figure 3.

First Simulation	Tikhonov	Gold	SSD	RL
Regularization parameter	$\lambda = 0.00065$	28921 iter.	$P = 0.81$	270 iter.
calculation time in ms	2.8	889	3.2	101
Tanimoto distance (Eqn. 26)	0.0133	0.0037	0.00089	0.0509

ChemPhysChem

Research Article
doi.org/10.1002/cphc.202200012

**Chemistry
Europe**

European Chemical
Societies Publishing

SSD, on the contrary, leads to a DRT spectrum that resembles the theoretical DRT outcome very well. All three peaks are sufficiently resolved, and no artifacts or oscillations are apparent. This finding is supported by very low ν values for the spectrum ($\nu < 0.2$) and the smallest Tanimoto distance with only $8.9 \cdot 10^{-4}$. Based on the DRT data, the impedance can be recalculated easily. The respective spectra are shown in the Supporting Information (7). In summary, the SSD and the Gold algorithm achieve DRT spectra that are closer to the optimal DRT spectrum than the DRT solution of the Tikhonov regularization.

The calculation times for Tikhonov and SSD are significantly shorter than for the RL and Gold algorithms. The main reason is that RL and Gold are iterative algorithms that require many iterations, whereas Tikhonov and SSD find a local minimum after a few iterations. The Gold algorithm has a much higher computation time than Richardson-Lucy because it needs more iterations to find an optimal minimum. The calculation time per iteration of Gold and RL is very similar. In the Experimental Section, additional calculation details are shown.

We further investigated the effect of increased Gaussian distributed error on the performance of all four algorithms. The respective results can be found in the Supporting Information (7). In these investigations, all algorithms compute DRT spectra that are similar to the results of Figure 3. Hence, the increased error has only minor effects on the algorithms. However, sightly increased Tanimoto distances and μ and ν values can be found.

In Figure 4, the results for the investigation of the second simulation setup are shown. The average ν values are much higher for the second simulation than for the first simulation, regardless of the used algorithm. These increased values are caused by a more complicated DRT due to more various exponents P. Again, when using the real impedance part for calculating the DRT spectra, lower μ values result. Besides, decreased RICV values can be found for utilizing the real part instead of the imaginary impedance part. ν, on the other hand, shows smaller values when the imaginary part is considered. Only for the Richardson-Lucy algorithm, the minimum of ν shows a lower value for the real part.

The resulting minima of all graphs of the Gold deconvolution and the Tikhonov regularization are much broader and have larger absolute values than for the first simulation setup. This effect can be explained by higher resistances within the investigated impedance simulation. As before, the μ values for the Tikhonov regularization are lower than for the Gold deconvolution, but the Gold deconvolution leads to lower ν values.

Due to the different exponential CPE factors for the second simulation setup, the respective theoretical DRT spectrum shows peaks of various widths (cf. Figure 1). Hence, ν and μ also show significantly broader minima and higher values for the Sparse Spike deconvolution. The qualitative course of the individual variables as a function of the respective regularization parameter is nevertheless comparable to the results of the first simulation (cf. Figure 2). A remarkably good agreement of the minima of all three variables (RICV, ν, and μ) is again apparent for the Sparse Spike deconvolution. However, the SSD

shows slightly higher ν values than the Gold algorithm and slightly lower values than the Tikhonov algorithm.

Like for the other algorithms, the RL algorithm shows higher ν and μ values with broader minima than for the first simulation. The low ν values for iterations between 10^3 and 10^4 show that the DRT is close to the optimal DRT, but the high μ values indicate DRT spectra leading to impedance spectra far from the optimum. With a $\mu > 1$ for all iterations, the Richardson-Lucy algorithm again proved unsuitable for solving the DRT problem.

For the SSD, Gold, and Tikhonov method, the RICV method is well suited for determining the regularization parameter that yields the lowest μ. For the RL algorithm, on the other hand, the RICV is insufficient to find an appropriate minimum for ν.

From Table 3, it is evident, that each algorithm has a higher Tanimoto distance than for the first simulation (cf. Table 2). Like the increased ν values, this effect is caused by a more complicated DRT than for the first impedance simulation. Overall the Tikhonov regularization has the highest Tanimoto distance and the Gold algorithm shows the lowest Tanimoto distance. The Tanimoto distances of the SSD and RL algorithm are similar. The computation times for the different algorithms show the same tendency as for the first simulation (cf. Table 3).
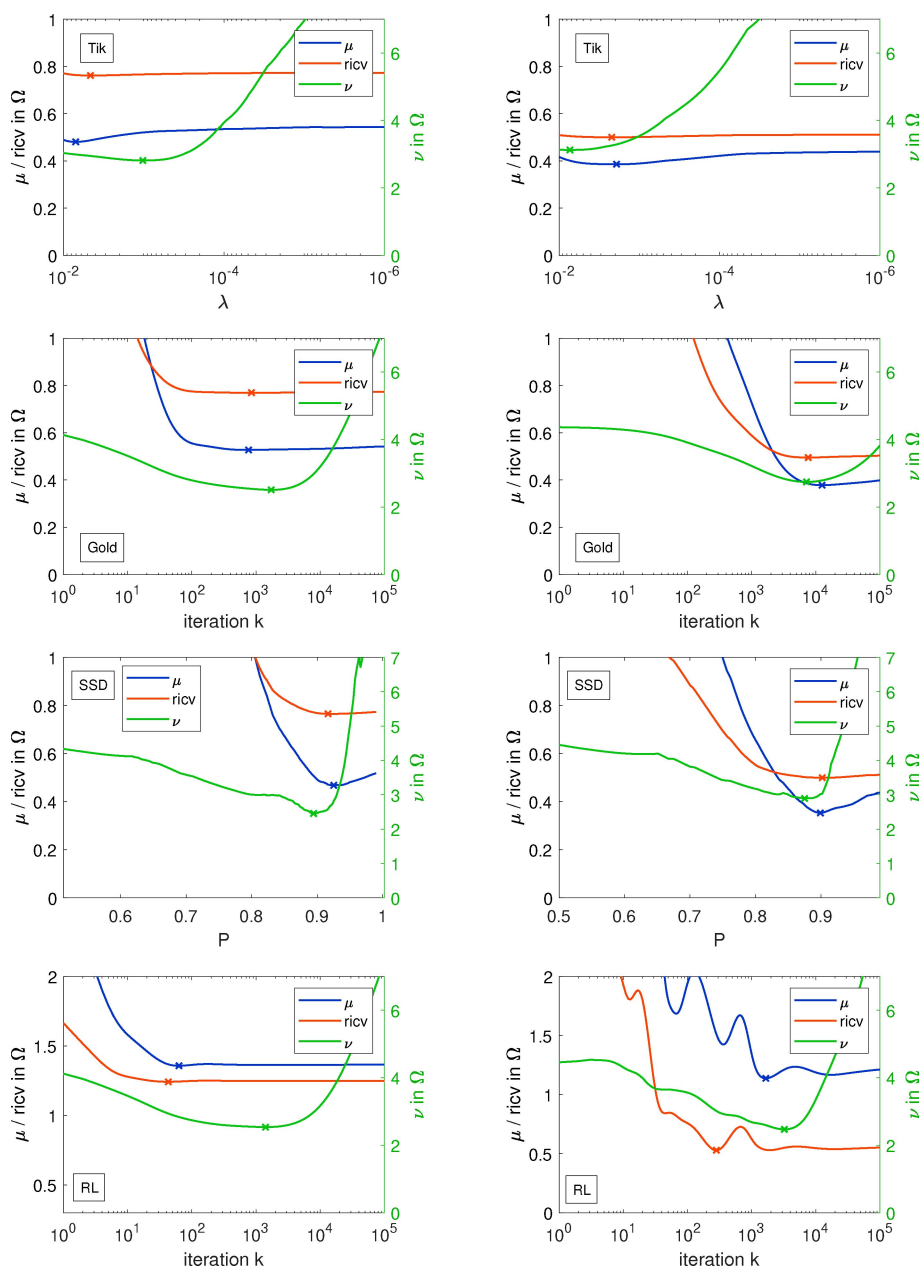
Figure 5 compares the respective DRT spectra at optimal RICV conditions with the theoretical optimum. Here, it can be seen that no regularization can simultaneously resolve both the spiky peak at $\tau \approx 0.02$ s and the broad peaks at higher time constants. Remarkably, all graphs own an additional small peak at $\tau \approx 2000$ s. Since all regularizations used the same erroneous data set, this peak is probably due to errors within the impedance simulation.

Despite the well-chosen regularization parameter λ, the Tikhonov regularization results in significant differences from the optimal spectrum. The sharp peak is insufficiently resolved, while the broad peaks split into multiple signals. In addition, the peak shape of the single peaks is far away from the expected peak form caused by a ZARC-element. Other authors also showed and discussed this behavior.[59] To get suitable DRT spectra, the Tikhonov regularization is improvable by modifying the minimization. However, these modifications probably lead to additional unwanted smoothing or additional regularization parameters (e.g., by adding radial basis functions with a shape factor).[37] Also, the usage of alternative functions like a Gaussian distribution leads to unwanted peak shapes.[60] Accordingly, the standard Tikhonov regularization is not a suitable method for generating non-negative DRT results with sharp and broad peaks at the same time.

Table 3. Regularization parameters, calculation times, and Tanimoto distances to the optimal DRT for each DRT calculated by the various algorithm and shown in Figure 5.

Second Simulation	Tikhonov	Gold	SSD	RL
Regularization parameter	$\lambda = 0.0022$	7649 iter.	$P = 0.902$	3247 iter.
calculation time in ms	2.7	347	3.7	128
Tanimoto distance (Eqn. 26)	0.211	0.156	0.174	0.180

ChemPhysChem

Research Article
doi.org/10.1002/cphc.202200012

**Chemistry
Europe**

European Chemical
Societies Publishing

Figure 4. ν and μ plotted against the regularization parameter for the second simulation, computed with different algorithms. Each row represents one algorithm. From top to bottom the algorithms are: Tikhonov, Gold, SSD, Richardson-Lucy. The first column used the imaginary part (equation 10) and the second used the real part (equation 9) for the calculation.
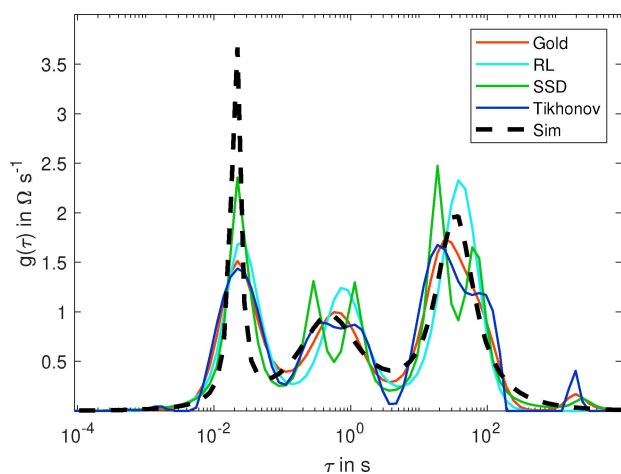
The Gold deconvolution is very well suited for determining DRT spectra because this deconvolution can lead to non-negative DRT results without using any constraints. Nevertheless, the sharp peak in Figure 5 is insufficiently resolved. The broad peaks, on the contrary, have almost the optimal shape. Overall, the Gold deconvolution leads nearly to a correct number of distinguishable peaks.

Also, the Richardson-Lucy method leads to non-negative results, and the peak shapes appear acceptable. Nevertheless, the corresponding μ is much higher than for the further algorithms. Therefore, it can be assumed that the DRT is oversimplified and leads to wrong parameters for the ZARC-

elements. Additionally, the minima of μ, ν, and RICV lie at very different iteration numbers.

The chosen P in the Sparse Spike deconvolution yields a good approximation of the large peak at low time constants. Unfortunately, the optimal regularization parameter, indicated by the RICV method, causes a splitting of the broader peaks into doublets. This way, the spectrum is clearly overfitted for higher time constants.

Nevertheless, the deficient DRT spectra (high ν) computed with the Tikhonov regularization, the Gold algorithm, or the SSD can still reproduce good impedance spectra (low μ). Accordingly, the defects in the DRT have only a slight influence

ChemPhysChem

Research Article
doi.org/10.1002/cphc.202200012

**Chemistry
Europe**
European Chemical
Societies Publishing

Figure 5. DRT spectra of all algorithms for the first simulation setup when the RICV is used for determining the regularization parameter. All DRT spectra were calculated from the real impedance part.

on the recalculation of impedance data. This effect is shown more in detail in the Supporting Information in Figures S1 and S2 for the first simulation and in Figures S3 and S4 for the second simulation. Even the additional peak splitting at higher time constants for the SSD and the Tikhonov regularization has no noticeable effect on the recalculated Nyquist plots. Only for the Richardson-Lucy method, larger deviations appear in the range of low frequencies. These, in turn, lead to the already mentioned high μ values.

The results for the second simulation show that the Sparse Spike deconvolution leads to a DRT with six peaks that strongly deviate from the optimal DRT spectrum. Unlike the other algorithms, which regularize the second norm of the DRT or are based on early stopping, the SSD regularizes the DRT by the parameter P. Here, the regularization parameter P corresponds directly to the exponents of the ZARC-elements P_i. If all P_i are equal, the searched peak function can, therefore, directly be used as an impulse function, and the Sparse Spike deconvolution leads to much better results than the other algorithms, as we showed for the first simulation. Consequently, we further investigated and improved the SSD.

The main problem of the SSD is that most experimental impedance spectra reflect multiple ZARC-elements with varying exponent values. Figure S10 in the Supporting Information shows the influence of various regularization parameters P on the DRT results for the second simulation. Unfortunately, every point in the deconvolution has the same impulse function. Hence, a low value for P leads to a good resolution of the broadest peak while simultaneously underfitting the further peaks. A high P value, on the other hand, yields a suitable resolution of the sharp peak while overfitting the remaining peaks. This problem can be overcome by using m separated regularization parameters instead of just one parameter. This way, we introduce the Separated Sparse Spike deconvolution (SSSD), which replaces the regularization parameter with a regularization vector.

3.3. Separated Sparse Spike Deconvolution

In the novel Separated Sparse Spike deconvolution, the regularization parameter P is substituted by a regularization vector **P** with M elements. Herein, M is the number of data points within the experimental impedance spectrum that will be deconvoluted. Zhang et al. introduced in a comparable approach a regularization vector for the Tikhonov regularization.[44] Following this work, we call the vector distribution of regularization factor (DRF).

Analogous to the previous SSD in equation 22, we now estimate for each regularization parameter P_m an impulse function $g_{i,m}$ which is given by,

$$g_{i,m}(P_m) = \frac{1}{2\pi} \frac{\sin(P_m \pi)}{\cosh(P_m(\ln(\tau_i) - \ln(\tau_m))) + \cos(P_m \pi)}, \qquad (27)$$

with $0 \leq P_m < 1$. The new normalized impulse function is given by,

$$G_{i,m}(P_m) = \frac{g_{i,m}(P_m)}{\sum_i (g_{i,m}(P_m))}. \qquad (28)$$

Herein, $G(\mathbf{P})$ is a matrix, in which each column m is a normalized impulse function with the regularization parameter P_m. A new minimization function is essential, which minimizes the DRF and equation 8 simultaneously. In this work, the minimization function is given by,

$$\min_{0 < \mathbf{P} < 1} \left(\left\| Z_{im} - A_{im} \cdot G(\mathbf{P}) \cdot c \right\|_2 + \left\| Z_{re} - A_{re} \cdot G(\mathbf{P}) \cdot c \right\|_2 + \frac{\left\| \ln(1 - \mathbf{P}) \right\|_2}{k} \right), \qquad (29).$$

where, c should be a vector, which defines the resistance for each time constant τ. Like in the other algorithms, the first two terms determine a DRT which can be used to recalculate a suitable impedance spectrum. The third term would lead to a DRF **P**, where every value would be zero. Thus, this term prevents overfitting of the impedance spectrum by reducing the possible exponents P of the ZARC-elements. This term needs to be scaled by k, which is the new regularization parameter in the SSSD. If a suitable k is found, the number of peaks in the DRF should be equal to the number of ZARC-elements in the simulation model (or to the correct number of ZARC-elements that describe the polarization behavior of experimental impedance data, respectively).

For each function call, c is calculated by,

$$\min_{c \geq 0} (\| Z_{re} - A_{re} \cdot G(\mathbf{P}) \cdot c \|_2). \qquad (30)$$

In the best case, c_i is zero for all time constants, except for the location of the ZARC-elements. If the DRF is calculated with equation 29 and the peaks c are calculated with equation 30, the DRT is calculated by,

$$g(\tau) = G(\mathbf{P}, \tau) \cdot c(\tau). \qquad (31)$$

ChemPhysChem

Research Article
doi.org/10.1002/cphc.202200012

**Chemistry
Europe**
European Chemical
Societies Publishing

In Figure 6, DRT spectra calculated with varying k values are presented. For $k = 0.1$, the third term of equation 29 has a too strong influence, and the spectrum is underfitted. For $k = 1000$, on the other hand, the spectrum is overfitted and contains too many peaks. For the values $k = 1$ and $k = 10$, the separated SSD leads to a DRT with the expected three peaks. Hence, an optimal k needs to be chosen, where the DRT is neither underfitted nor overfitted.
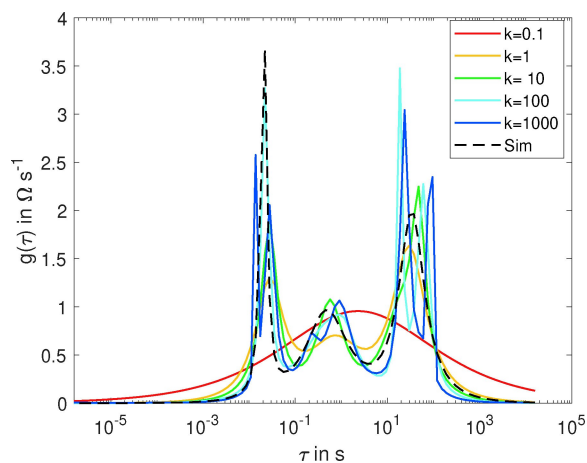
Figure 6. DRT spectra for the second simulation setup, calculated by the separated SSD for different regularization parameters k ($k = 0.1$ up to $k = 1000$).
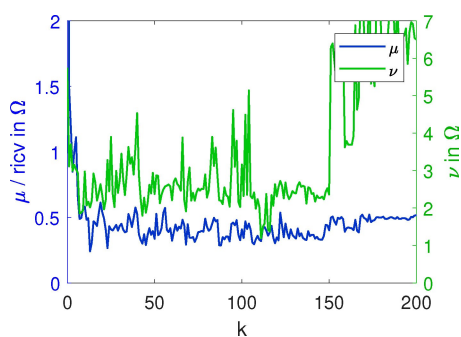
Figure 7. ν and μ, calculated using eqn. 24 and 25, for the separated SSSD. Both values plotted against the regularization parameter k.
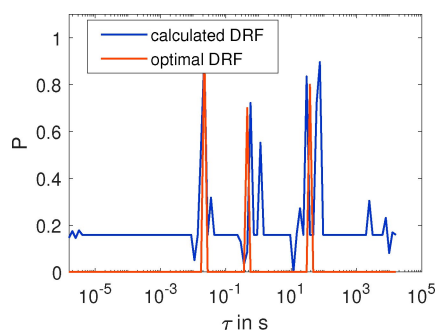
**Figure 8.** The optimal theoretical DRF, and the DRF calculated using equation 29 with $k = 111$. All plotted against τ.

Figure 7 depicts ν and μ for different k from 1 to 200. For $k \leq 8$, the increasing ν and μ indicate an underfitting, and for $k \geq 150$, the increasing ν with a constant μ indicates an overfitting. It can be seen that for each k, the minimization of the DRF has problems finding the global minimum and often gets stuck in local minima. Therefore, the results of ν and μ are very noisy. This problem is mainly due to too many variables within the DRF. Due to high number of variables, it is difficult to find an optimal solution and for each k, we got a computation time between 20 and 24 seconds. This shows that this algorithms is much slower than the algorithms studied beforehand (see Table 3). In Figure 7, a minimal ν was obtained for $k = 111$ with $\nu = 1.19$ and $\mu = 0.318$. The respective DRF is presented in Figure 8. Surprisingly, the calculated DRF does not match the expectation of the optimal DRF. The median of the DRF is about 0.16 instead of zero, which indicates an unfinished minimization. Many small peaks exist which have no impact on the spectra. Only five values are above the value 0.5 and show potential positions for DRT signals.

The corresponding DRT for $k = 111$ is shown in Figure 9. For the SSSD, we obtained a Tanimoto distance of 0.0273 which is much lower than for all other algorithms (see Table 3). The DRT spectrum of the SSSD algorithm fits the theoretical optimum much better than all DRT spectra of Figure 5. Due to the use of the DRF, the broad peaks are not split into multiple peaks and the sharp peak is well resolved simultaneously. Overall, the DRT of the separated SSD is almost optimal resolved, and no additional peaks are visible.

An additional advantage of this method is that the determination of the ZARC-parameters out of the DRT results is straightforward (cf. 7 in the Supporting Information).

For further investigation of the impact of divergent CPE exponents on the DRT outcome of the studied algorithms, we examined a fourth simulated impedance spectrum, which just contained the sharpest and the broadest peak of the second impedance simulation. Additionally, to examine the dependency between the regularization parameters and the magnitude, we reduced the resistances' magnitude by a factor of
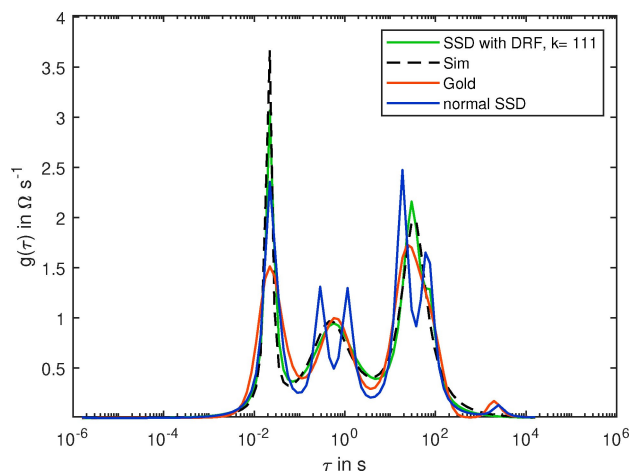
Figure 9. Best DRT results for the separated SSD, the Gold deconvolution and the normal SSD in comparison with the theoretical optimum.

Table 4. Parameters of the simulated ZARC-elements.

	R_1 in Ω	Q_1 in $\frac{s}{\sqrt{\Omega}}$	P_1	R_2 in Ω	Q_2 in $\frac{s}{\sqrt{\Omega}}$	P_2	R_2 in Ω	Q_2 in $\frac{s}{\sqrt{\Omega}}$	P_2
1st Setup	1.6	0.10	0.80	2.0	1.0	0.8	2	10	0.8
2nd Setup	2.0	0.01	0.95	3.0	0.1	0.7	4	6	0.8
3rd Setup (7)	1.6	0.10	0.80	2.0	1.0	0.8	2	10	0.8
4th Setup (7)	$2.0 \cdot 10^{-3}$	14.4	0.95	$3.0 \cdot 10^{-3}$	1930	0.7	0	0	0.0

1000. The results are presented in the Supporting Information (cf. section 7).

Besides the simulated data sets, we investigated an experimental impedance spectrum of a lithium-ion cell. The respective results can be found in the Supporting Information (cf. section 7). These results show that the SSSD is well suited to describe experimental impedance spectra as well. The SSSD even seems to calculate a superior DRT solution than the other algorithms.

Experimental Section

Simulation Parameters

All algorithms were tested and evaluated using simulated impedance data. In total, four different data sets were generated for this purpose. The impedance spectra differ in terms of their exact parametrization (resistance, CPE factors - cf. setup 1 vs. setup 2 in Table 4) and their error structure (cf. setup 1 vs. setup 3 in Table 5). The fourth setup differs in the equivalent circuit used for the simulation and in terms of the magnitude of the resistances and CPE parameters. The first three impedance simulations were computed based on three ZARC-elements, connected in series. For the fourth simulation, only two ZARC-elements were used. For all simulations, the impedance was simulated in a frequency range between 10^{-5} to 10^5 Hz with 10 points per frequency decade. The parameters of the respective passive elements are listed in Table 4. For the calculation of the impedance, equation 3 was used. In addition, we calculated for each simulated impedance setup the respective theoretical DRT spectrum, using equation 7. The theoretical DRT spectra were used to evaluate the results of the different DRT algorithms introduced in this work. Furthermore, optimal impedance data was recalculated from the theoretical DRT spectra. The optimal impedance spectra are needed to calculate the test value μ (cf. section 4.2).

Experimental impedance spectra of electrochemical systems are always erroneous. Therefore, the presented algorithms were tested on simulated data sets that were falsified by a Gaussian distributed error. The following equations were used to generate erroneous simulated data:

$$Z_{sim}'(\omega_i) = Z_{opt}'(\omega_i) + e_1' \cdot \left\| Z_{opt}(\omega_i) \right\|_2 \cdot \mathcal{N}(0,1) + e_2' \cdot \mathcal{N}(0,1) \tag{32}$$

Table 5. The variables for the error simulation of the impedance data.

	e_1'	e_2'	e_1''	e_2''	e_f
1st Setup	0.002	0.002	0.002	0.002	0.001
2nd Setup	0.008	0.008	0.008	0.008	0.002
3rd Setup (7)	0.010	0.020	0.010	0.020	0.001
4th Setup (7)	0.0	0.0	$3 \cdot 10^{-5}$	$3 \cdot 10^{-5}$	0.002

$$Z_{sim}''(\omega_i) = Z_{opt}''(\omega_i) + e_1'' \cdot \left\| Z_{opt}(\omega_i) \right\|_2 \cdot \mathcal{N}(0,1) + e_2'' \cdot \mathcal{N}(0,1) \tag{33}$$

Here, the real and imaginary parts were treated separately from each other. The variables e_1', e_2', e_1'' and e_2'' scale the error size. Each variable is multiplied by a normal distribution $\mathcal{N}$ with $\mu = 0$ and $\sigma = 1$. The second term is depending on the modulus of the impedance. Therefore, the errors are depending on the magnitude and are higher at lower frequencies.

Apart from the impedance, the frequency is also prone to errors and an additional error factor to the frequency is added by,

$$\omega_{sim}(i) = \omega_{opt}(i) \cdot (1 - e_f \cdot \mathcal{N}(0,1)). \tag{34}$$

Table 5 lists the variables for the error calculation.

Fitting Algorithm

To find the best solution for the Tikhonov regularization and the sparse spike deconvolution, we used the interior-point method of MatLab.[61] The maximum iteration number was 5000 and the maximum function tolerance was 10^{-15}. Generally, both algorithms stopped the minimization between 15 and 30 iterations. For the SSSD, we used a modified version of the particle swarm optimization of MatLab to find the optimal solution. The swarm size was set to 2000 with a maximum iteration of 300 and a maximum function tolerance of 10^{-9}. We also investigated optimizations with higher iteration numbers, but often a local minimum was found by about 100 iterations and only negligible changes were found for further iterations. The Gold algorithm and the Richardson-Lucy algorithm are iterative algorithms and hence do not need any further minimization algorithms.

All calculations were performed on an AMD Ryzen 7 3700X 8-Core Processor with 3.59 GHz.

4. Conclusion

In this work, we introduced three algorithms for the determination of DRT spectra from experimental impedance data and compared their performance to the often used Tikhonov regularization. The shown approaches are the Gold algorithm, the Richardson-Lucy algorithm, and the Sparse Spike deconvolution. Simulated impedance data sets have been used to compare the results of each algorithm to theoretical DRT spectra. For all algorithms, we used the RICV (Real-Imaginary-Cross-Validation) to estimate the optimal regularization parameter.

The comparison between the different algorithms showed that the DRT spectra of the Gold deconvolution are closer to the optimal DRT than the solutions calculated with the Tikhonov regularization. For the commonly used Tikhonov

ChemPhysChem

Research Article
doi.org/10.1002/cphc.202200012

Chemistry Europe
European Chemical
Societies Publishing

method, necessary boundaries and the penalty term, which reduces the norm of the DRT, prevent the formation of natural spectroscopic peaks. Especially, when the experimental impedance spectrum contains both sharp and broad peaks, the resulting DRT spectra of the Tikhonov regularization are poorly resolved. The iterative Richardson-Lucy algorithm requires no constraints and shows low iteration numbers, but the DRT results were insufficient and showed pronounced deviations from the theoretical optima. When all exponential ZARC-parameters P_i of the simulated system are close to each other, the Sparse Spike deconvolution (SSD) yields nearly optimal results. For exponents P_i, significantly deviating from each other, however, the SSD leads to overfitted DRT spectra.

Consequently, we substituted the regularization parameter of the SSD with a suitable regularization vector **P** and introduced the Separated Sparse Spike deconvolution (SSSD). This way, the simulated data could be deconvoluted into nearly optimal DRT spectra regardless of the variation of the ZARC-parameters P_i. However, the prerequisite for valid DRT results remains the determination of a suitable regularization parameter. Unfortunately, the presented Separated Sparse Spike deconvolution is accompanied by a high number of local minima. This effect is due to an extensive quantity of variables within the minimization. Nevertheless, the SSSD can calculate high qualitative DRT spectra, which are not achievable by a Tikhonov regularization. Hence, alternative minimization functions within the SSSD should be tested in future work to find stable global minima. Furthermore, we will publish a GUI concluding each algorithm after further development and optimizations.

Symbol and Description

Z	impedance
R_i	resistance of the ZARC-element i
C_i	capacitance of the ZARC-element i
P_i	exponent of the ZARC-element i
τ_i	time constant of the ZARC-element i
N	number of ZARC-elements
ω	angular frequency of the alternating excitation signal
τ	relaxation time
γ	distribution of relaxation time
A	convolution matrix
$\mathbf{x}$	solution of the ill-posed problem
$\mathbf{x}_{best}$	best solution of the ill-posed problem
ν	discrepancy to the optimal DRT
μ	discrepancy to the error-free EIS data
g	impulse function for the SSD
c	distribution of regularization factor

Abbreviations and Description

CNLS	Complex nonlinear least-squares regression
EC	Equivalent circuit
EIS	Electrochemical impedance spectroscopy
DRT	Distribution of relaxation time
DRF	Distribution of regularization factor
RICV	Re—Im cross-validation
SSD	Sparse spike deconvolution
SSSD	Separated sparse spike deconvolution
CPE	Constant Phase Element
ZARC	A Arc-shaped impedance Z
	Generally, a resistance and a CPE connected in parallel

Conflict of Interest

The authors declare no conflict of interest.

Data Availability Statement

The data that support the findings of this study are available from the corresponding author upon reasonable request.

[1] Claude Gabrielli, PhD thesis, Pierre and Marie Curie University, **1998**.
[2] D. A. Harrington, P. Van Den Driessche, *Electrochim. Acta* **2011**, *56*, 8005–8013.
[3] B. Andreaus, A. J. McEvoy, G. G. Scherer, *Electrochim. Acta* **2002**, *47*, 2223–2229.
[4] E. B. Easton, P. G. Pickup, *Electrochim. Acta* **2005**, *50*, 2469–2474.
[5] A. K. Manohar, O. Bretschger, K. H. Nealson, F. Mansfeld, *Bioelectrochemistry* **2008**, *72*, 149–154.
[6] Z. He, F. Mansfeld, *Energy Environ. Sci.* **2009**, *2*, 215–219.
[7] P. Izadi, M. N. Gey, N. Schlüter, U. Schröder, *iScience* **2021**, *24*, DOI 10.1016/j.isci.2021.102822.
[8] W. Choi, H. C. Shin, J. M. Kim, J. Y. Choi, W. S. Yoon, *J. Electrochem. Sci. Technol.* **2020**, *11*, 1–13.
[9] N. A. Cañas, B. Hirose, B. Pascucci, N. Wagner, K. A. Friedrich, R. Hiesgen, *Electrochim. Acta* **2013**, *97*, 42–51.
[10] P. Suresh, A. K. Shukla, N. Munichandraiah, *J. Appl. Electrochem.* **2002**, *32*, 267–273.
[11] Y. Huang, H. Shih, H. Huang, J. Daugherty, S. Wu, S. Ramanathan, C. Chang, F. Mansfeld, *Corros. Sci.* **2008**, *50*, 3569–3575.
[12] Y. J. Tan, S. Bailey, B. Kinsella, *Corros. Sci.* **1996**, *38*, 1545–1561.
[13] L. Wu, Y. Ogawa, A. Tagawa, *J. Food Eng.* **2008**, *87*, 274–280.
[14] M. Adachi, M. Sakamoto, J. Jiu, Y. Ogata, S. Isoda, *J. Phys. Chem. B* **2006**, *110*, 13872–13880.
[15] J. Illig, PhD thesis, Karlsruhe Institute of Technology, **2014**.
[16] S. Havriliak, S. Negami, *Polymer* **1967**, *8*, 161–210.
[17] N. Schlüter, T. Bergmann, S. Ernst, U. Schröder, *ChemElectroChem* **2021**, *8*, 1167–1182.

[18] Z. Kerner, T. Pajkossy, *J. Electroanal. Chem.* **1998**, *448*, 139–142.

[19] F. Dion, A. Lasia, *J. Electroanal. Chem.* **1999**, *475*, 28–37.

[20] S. Holm, T. Holm, Ø. G. Martinsen, *PLoS One* **2021**, *16*, DOI 10.1371/journal.pone.0248786.

[21] B. Y. Chang, *J. Electrochem. Sci. Technol.* **2020**, *11*, 318–321.

[22] J. R. Macdonald, *Electrochim. Acta* **1990**, *35*, 1483–1492.

[23] D. Ritzmann, P. S. Wright, W. Holderbaum, B. Potter, *IEEE Trans. Instrum. Meas.* **2016**, *65*, 2204–2213.

[24] A. Al-Ali, A. Elwakil, B. Maundy, D. Westwick, *AEU - Int. J. Electron. Commun.* **2020**, *123*, 153301.

[25] M. A. Danzer, *Batteries* **2019**, *5*, 1–16.

[26] E. von Schweidler, *Ann. Phys.* **1907**, *24*, 711.

[27] L. Landweber, **2009**, *73*, 615–624.

[28] R. M. Fuoss, J. G. Kirkwood, *J. Am. Chem. Soc.* **1941**, *63*, 385–394.

[29] E. Ivers-Tiffée, A. Weber, Evaluation of electrochemical impedance spectra by the distribution of relaxation times, **2017**.

[30] N. Schlüter, S. Ernst, U. Schröder, *ChemElectroChem* **2019**, *6*, 6027–6037.

[31] H. Schichlein, A. C. Müller, M. Voigts, A. Krügel, E. Ivers-Tiffée, *J. Appl. Electrochem.* **2002**, *32*, 875–882.

[32] B. A. Boukamp, *Electrochim. Acta* **2015**, *154*, 35–46.

[33] J. Macutkevic, J. Banys, A. Matulis, *Nonlinear Anal. Model. Control* **2004**, *9*, 75–88.

[34] S. Eichstädt, F. Schmähling, G. Wübbeler, K. Anhalt, L. Bünger, U. Krüger, C. Elster, *Metrologia* **2013**, *50*, 107–118.

[35] R. Gold, *An iterative unfolding method for response matrices*, Argonne National Laboratory, Illinois, **1964**.

[36] A. L. Gavrilyuk, D. A. Osinkin, D. I. Bronin, *Electrochim. Acta* **2020**, *354*, 136683.

[37] T. H. Wan, M. Saccoccio, C. Chen, F. Ciucci, *Electrochim. Acta* **2015**, *184*, 483–499.

[38] N. Schlüter, S. Ernst, U. Schröder, *ChemElectroChem* **2020**, *7*, 3445–3458.

[39] M. Saccoccio, T. H. Wan, C. Chen, F. Ciucci, *Electrochim. Acta* **2014**, *147*, 470–482.

[40] G. H. Golub, P. C. Hansen, D. P. O'Leary, *SIAM J. Matrix Anal. Appl.* **1999**, *21*, 185–194.

[41] A. L. Gavrilyuk, D. A. Osinkin, D. I. Bronin, *Russ. J. Electrochem.* **2017**, *53*, 575–588.

[42] A. Kulikovsky, *Phys. Chem. Chem. Phys.* **2020**, *22*, 19131–19138.

[43] A. Mertens, J. Granwehr, *J. Energy Storage* **2017**, *13*, 401–408.

[44] Y. Zhang, Y. Chen, M. Li, M. Yan, M. Ni, C. Xia, *J. Power Sources* **2016**, *308*, 1–6.

[45] M. Morh, V. Matouek, *J. Comput. Appl. Math.* **2011**, *235*, 1629–1640.

[46] M. Fuhry, L. Reichel, *Numer. Algor.* **2012**, *59*, 433–445.

[47] P. Bandžuch, M. Morháč, J. Krištiak, *Nucl. Instrum. Methods Phys. Res. Sect. A* **1997**, *384*, 506–515.

[48] T. Zhou, S. C. Popescu, K. Krause, R. D. Sheridan, E. Putman, *ISPRS J. Photogramm. Remote Sens.* **2017**, *129*, 131–150.

[49] M. Morháč, J. Kliman, V. Matoušek, M. Veselský, I. Turzo, *Nucl. Instrum. Methods Phys. Res. Sect. A* **1997**, *401*, 385–408.

[50] Y. Sui, J. Ma, *Geophysics* **2020**, *85*, V481–V496.

[51] L. Yuan, J. Sun, L. Quan, H.-Y. Shum, *ACM Trans. Graph.* **2007**, *26*, 1.

[52] Y. W. Tai, M. S. Brown, *IEEE Trans. Pattern Anal. Mach. Intell.* **2011**, *33*, 161–183.

[53] M. Morh, V. Matouek, *J. Comput. Appl. Math.* **2011**, *235*, 1629–1640.

[54] R. Fernandes, H. Lopes, M. Gattass, **2017**, *14*, 2240–2244.

[55] L. Wang, Q. Zhao, J. Gao, Z. Xu, M. Fehler, X. Jiang, *Geophysics* **2016**, *81*, V169–V182.

[56] K. F. Kaaresen, *IEEE Trans. Signal Process.* **1998**, *46*, 609–624.

[57] C. Dossal, S Mallat, *In Proceedings of SPARS* **2005**, 123–126.

[58] A. H. Lipkus, *J. Math. Chem.* **1999**, *26*, 263–265.

[59] B. A. Boukamp, *Electrochim. Acta* **2017**, *252*, 154–163.

[60] K. S. Cole, R. H. Cole, *J. Chem. Phys.* **1941**, *9*, 341–351.

[61] R. H. Byrd, J. C. Gilbert, J. Nocedal, *Math. Program. Ser. B* **2000**, *89*, 149–185.